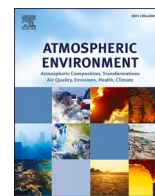




Contents lists available at ScienceDirect

# Atmospheric Environment

journal homepage: [www.elsevier.com/locate/atmosenv](http://www.elsevier.com/locate/atmosenv)

## Source attribution of nitrogen oxides across Germany: Comparing the labelling approach and brute force technique with LOTOS-EUROS

M. Thürkow<sup>a,\*</sup>, S. Banzhaf<sup>a</sup>, T. Butler<sup>a,c</sup>, J. Pültz<sup>a</sup>, M. Schaap<sup>a,b</sup><sup>a</sup> Institute of Meteorology, Freie Universität Berlin, Carl-Heinrich-Becker-Weg 6-10, 12165, Berlin, Germany<sup>b</sup> TNO, Department Climate Air and Sustainability, Princetonlaan 6, 3584 CB, Utrecht, the Netherlands<sup>c</sup> IASS, Institute for Advanced Sustainability Studies, Berliner Strasse 130, 14467, Potsdam, Germany

### HIGHLIGHTS

- Two techniques for source attribution of nitrogen oxides were successfully applied.
- Upscaling the impacts of scenarios under- or overexplains the total concentrations.
- Differences between methodologies are largest for smaller emission source sectors.
- Applying the brute force technique to single sectors for NO should be avoided.

### ARTICLE INFO

#### Keywords:

Source attribution  
 Labelling  
 Brute force  
 Chemistry transport model  
 Nitrogen oxides

### ABSTRACT

Millions of people are exposed to enhanced levels of nitrogen dioxide in urbanized areas, leading to severe health effects. Moreover, nitrogen oxides contribute to the formation of ozone and particulate matter, and as such have wider health related impacts. A substantial reduction of nitrogen oxides may offer considerable health benefits for the human society. As a first step, this requires a detailed understanding of source sector contributions to nitrogen oxide levels. Whereas many regions have information on the local (traffic) contributions, the source contributions to the rural and urban background levels are commonly not available. In this study we compared and evaluated the results of two source attribution techniques to quantify the contribution of 5 source sectors to background nitrogen oxide levels across Germany. The results of a labelling technique were compared to brute force simulations with variable emission reduction percentages. The labelled NO<sub>2</sub> source contributions of the main sectors averaged for all urban background stations are road transport (45 ± 5%), non-road transport (24 ± 6%), energy & industry (20 ± 3%), households (10 ± 6%), and the remaining source sectors (1 ± 1%). For the brute force technique, the explained mass differs from the unperturbed baseline concentration after scaling the impact of each sensitivity simulation to 100%. The attributed concentration of NO<sub>2</sub> is lower in urban background areas (−3 ± 5%) and larger in the rural background (4 ± 6%) than that of the labelling. Largest deviations up to −15% are calculated for the major cities along the Rhine and Main. The annual average overestimation for NO is about 53 ± 24% for urban and 40 ± 26% for rural background sites based on a 20% reduction of emissions. On shorter time scales the differences are larger. These deviations are caused by (the lack of) regime changes in the titration of ozone, most notably present at ozone-limiting conditions during nocturnal winter periods. As a consequence, the differences between the methodologies are larger for smaller emission reduction percentages applied in the brute force technique. Similarly, for small-sized emission source sectors larger deviations were found compared to large-sized sector categories. Hence, applying the brute force technique for the source attribution for a single sector should be avoided as there is no way to verify for consistency and quantify the error for the sector and total explained contribution. We recommend applying the labelling approach to estimate sector contributions in forthcoming studies for nitrogen oxides.

\* Corresponding author.

E-mail address: [markus.thuerkow@met.fu-berlin.de](mailto:markus.thuerkow@met.fu-berlin.de) (M. Thürkow).

<https://doi.org/10.1016/j.atmosenv.2022.119412>

Received 16 March 2022; Received in revised form 21 September 2022; Accepted 25 September 2022

Available online 30 September 2022

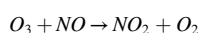
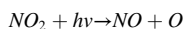
1352-2310/© 2022 The Authors. Published by Elsevier Ltd. This is an open access article under the CC BY license (<http://creativecommons.org/licenses/by/4.0/>).

## 1. Introduction

Poor air quality is one of the key challenges of the 21<sup>st</sup> century facing the environmental community (Lim et al., 2012). Nitrogen oxides (NO<sub>x</sub> = NO + NO<sub>2</sub>) belong to the main pollutants causing a range of negative effects on human wellbeing. Numerous studies have confirmed that exposure to nitrogen dioxide (NO<sub>2</sub>) leads to increased mortality (Fischer et al., 2015; Beelen et al., 2014; Raaschou-Nielsen et al., 2012). In Germany, exposure to NO<sub>2</sub> is a major health concern with an estimated annual number of 13,100 premature deaths (EEA, 2018). In addition, nitrogen oxides contribute to the formation of ozone (O<sub>3</sub>) and particulate matter (PM), and as such are relevant to wider health implications (Kampa and Castanas, 2008). Additionally, nitrogen oxides contribute to acidification and eutrophication of soils and water bodies and, consequently, to a loss of biodiversity in terrestrial and aquatic ecosystems (Fowler et al., 2013). Exceedances of limit values usually only occur in high populated areas near busy roads. The annual limit value of 40 µg/m<sup>3</sup> for NO<sub>2</sub> as introduced by the European Ambient Air Quality Directive (European Council, 2008) is currently exceeded by about 39% at German traffic sites (UBA, 2019). The hourly mean limit value of 200 µg/m<sup>3</sup> for NO<sub>2</sub> has not been exceeded in Germany recently (UBA, 2019).

Major emission sources and formation processes of nitrogen oxides are well documented. Anthropogenic emissions of nitrogen monoxide (NO) mostly form at high temperatures during (incomplete) combustion processes, such as from traffic, shipping, energy production, or residential combustion (Granier et al., 2011; Vestreng et al., 2009). In addition, smaller emission sources derive from agricultural soils, lightning and geogenic sources (Fowler et al., 2013). In the presence of ozone, NO is oxidized to NO<sub>2</sub>. As such, near their sources NO emissions disturb the photochemical equilibrium of the Leighton cycle (Finlayson-Pitts and Pitts, 2000; Leighton, 1961) and cause a titration of ozone levels (Eq. 1).

### Eq. 1 Leighton cycle



Occasionally, an excess of fresh NO may titrate all ozone away and a build-up of NO occurs. Such events occur mostly under low ventilation conditions during winter in high emission areas such as urban centers (Finlayson-Pitts and Pitts, 2000; Leighton, 1961). In presence of ozone, NO<sub>2</sub> can be oxidized to nitric acid in several hours with subsequent particulate nitrate formation in presence of ammonia or sea salt (Schaap et al., 2004).

To further improve the ambient air quality it is important to know the extent to which the different anthropogenic activities contribute to the NO<sub>2</sub> exposure (Belis et al., 2020). Source attribution is a process of tracing pollution levels back to its origin. Increments between roadside and urban background stations and/or urban street canyon modelling are often used to quantify local contributions, with the limitation that no source attribution for the urban background is obtained (Thunis, 2018). Hence, a source attribution of background levels is commonly not available for city, municipal and state authorities. Rural and urban background levels can be assessed using chemical transport model (CTM) simulations, which are applied in an increasing number of studies (SenStadt, 2019; UBA, 2019). When applying CTMs for source attribution two main methods can be considered: (1) source apportionment approaches, also known as the labelling (Kranenburg et al., 2013) or tagging technique (Butler et al., 2018; Wang et al., 2009; Wagstrom et al., 2008), based on the calculation of a mass concentration and (2) brute force algorithms which are based on sensitivity simulations perturbing the emission input data (Thunis et al., 2019; Clappier et al., 2017). As both methods differ intrinsically, their target quantities can be

distinguished as contributions (labelling) and impacts (brute force) (Clappier et al., 2017). Numerous studies assessed the source attribution for particulate matter or ozone, either applying the labelling approach (Timmermans et al., 2020, 2017; Lupaşcu and Butler, 2019; Banzhaf et al., 2015; Curier et al., 2014; Hendriks et al., 2013; Schaap et al., 2013) or the brute force technique (Van Dingenen et al., 2018; Huang et al., 2018; Thunis et al., 2018; Amann et al., 2011). Although the application of the labelling technique to nitrogen oxides has implicitly been performed in these studies, they have hardly been the main focus and comparing the labelling and brute force techniques has received little attention.

Several studies indicate that the brute force technique tends to fail for the determination of contributions (Kwok et al., 2015), which can be related to indirect effects such as oxidant-limited reaction processes (Koo et al., 2009). In case of non-linear relations, the estimated total impact from sensitivity simulations may not correspond to the total mass concentration of the base simulation (Koo et al., 2009). Large inconsistencies have been reported for ozone by e.g. Mertens et al. (2018), who showed that ozone source attribution using a perturbation approach could differ by up to a factor of 4 compared with a tagging approach. Butler et al. (2020) combined both perturbation and tagging approaches for ozone to show that the ozone production efficiency of precursors from unperturbed emission sectors increased to partially compensate for reduced emissions of ozone precursors by a given sector. In case of nitrogen oxides, non-linear behavior can be expected with respect to photochemistry and ozone titration effects (Finlayson-Pitts and Pitts, 2000; Leighton, 1961), which are highly sensitive to meteorological conditions (Munir, 2016). Hence, as there is no standardized method and/or definition available on how to conduct source attribution studies for background nitrogen oxide levels, we aim to compare the results of the labelling and brute force approach in this study.

This study aims to answer the following research questions: (1) To what extent are contributions by the brute force technique and the labelling approach comparable to each other for the source attribution of nitrogen oxides? (2) Does the application of sensitivity simulations reveal non-linear impacts in the concentration with respect to varying nitrogen oxide emission reduction levels? (3) Up to what application range are sensitivity simulations suitable to determine contributions for nitrogen oxide source attribution purposes? To answer these research questions, we conducted a source attribution study for Germany by performing air pollution simulations using the LOTOS-EUROS CTM for January 1<sup>st</sup> to December 31<sup>st</sup>, 2018. In section 2 we describe the labelling and brute force approach taken in this study as well as the approach for comparison. In section 3 the results are provided in terms of distributions and station typology across Germany. Finally, the results are discussed and put in broader perspective in section 4.

## 2. Methodology

Below, we first provide a description of the LOTOS-EUROS CTM and the model set-up. Next, we introduce the labelling and brute force concepts, which have been applied to evaluate their ability for source attribution purposes of nitrogen oxides. The last subsection details the methodology used to evaluate the differences between the methods.

### 2.1. Chemical transport modelling

For this study, the LOTOS-EUROS chemical transport model (CTM) version 2.2 was employed. The model has a long application history in Europe (Manders et al., 2017) and is part of the regional ensemble of the Copernicus Atmospheric Monitoring Service (CAMS). Within CAMS the model is applied operationally to provide air quality forecasts and analyses for the European region (Marécal et al., 2015), including particulate matter source attribution information using a labelling approach (Pommier et al., 2020). Air quality simulations with the LOTOS-EUROS CTM are performed on an Eulerian grid of variable resolution in the

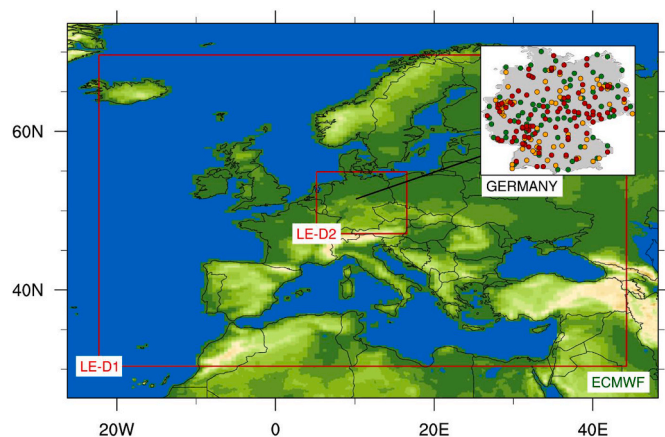


**Fig. 1.** Domain configuration of the model area. Two zooming domains are used for the LOTOS-EUROS CTM simulations (red). Meteorological input data are provided by the ECMWF model (green). The investigation area of Germany is highlighted on the right-hand side with dots indicating the German monitoring sites (urban background: red, sub-urban background: orange and rural background: green). (For interpretation of the references to color in this figure legend, the reader is referred to the Web version of this article.)

horizontal and terrain following coordinates in the vertical (Manders et al., 2017), with horizontal advected air pollutants calculated according to a monotonic advection scheme developed by Walcek (2000). The gas-phase chemistry is described by the TNO CBM-IV scheme, a modified implementation based on the scheme by Whitten et al. (1980). Aerosol chemistry related processes are handled by the thermodynamic equilibrium module ISORROPIA-II (Fountoukis and Nenes, 2007), while the cloud chemistry sulfate formation is explicitly treated according to the algorithm developed by Banzhaf et al. (2012). To handle dry deposition within gas phase, the DEPAC module (DEPosition of Acidifying Compounds) is applied (Wichink Kruit et al., 2012; Van Zanten et al., 2010), with the derivation of particles following the scheme of Zhang et al. (2001). The wet deposition is solved as described in the study of Banzhaf et al. (2012). More detailed information with full process descriptions and implementation examples of the LOTOS-EUROS CTM, are provided by Manders et al. (2017) and references therein.

The model simulations, covering Europe and the target area of Germany, were conducted by applying a one-way nesting approach (Fig. 1). The outer domain with a horizontal grid resolution of  $0.5^\circ$  longitude to  $0.25^\circ$  latitude ( $\sim 28 \times 32 \text{ km}^2$ ) was used to encompass the impacts of long-range transport on air quality in Germany and extends from  $22^\circ\text{W}$ - $44^\circ\text{E}$  to  $31^\circ\text{N}$ - $69^\circ\text{N}$ . The inner domain ( $0.125^\circ$  longitude  $\times$   $0.0625^\circ$  latitude,  $\sim 7 \times 8 \text{ km}^2$ ) focuses on Germany, and covers parts of the neighboring countries, e.g. the Netherlands, Belgium, Luxembourg, and Poland. To determine the vertical layering of the model system, we used a dynamic mixed layer approach (Manders et al., 2017). Following the operational set-up of the LOTOS-EUROS, meteorological input data of the IFS (Integrated Forecasting System) is provided by the ECMWF

(Flemming et al., 2009). We performed model simulations for the period of January 1<sup>st</sup> to December 31<sup>st</sup>, 2018, plus one month of spin-up time.

For Germany, the official reported anthropogenic emission inventory, gridded using the GRETA (Gridding Emission Tool for ArcGIS, Schneider et al. (2016)) system, was applied. The CAMS emissions developed by the TNO for 2015 (CAMS-RWC-SNAP78.2015), were taken for the rest of Europe. Time profiles for individual source sectors represent the temporal variation, which break down the annual emission totals based on monthly, daily, and hourly scaling factors. Temporal variability for residential combustion emissions was considered using a heating degree days approach to allow for different heating demands depending on meteorological conditions following Mues et al. (2014). Except for road transport, we used 97% for NO and 3% for NO<sub>2</sub> for the direct emissions. For road transport the direct NO<sub>2</sub> emission percentage was set to 20%, which is in agreement with recent studies (Kimbrough et al., 2017; Richmond-Bryant et al., 2017). Information on wild fire emissions were taken from the CAMS fire product (Kaiser et al., 2012). C-IFS (Integrated Forecasting System including Chemistry, Marécal et al. (2015)) distributions were used as input for chemical boundary conditions for the European domain.

## 2.2. Simulation strategy for source attribution

The LOTOS-EUROS CTM contains a labelling module for source attribution, to determine the origin of particulate matter compounds and their related precursors (Kranenburg et al., 2013). A pre-defined number of emission sectors or regions can be given a label which are traced during the model simulation of the LOTOS-EUROS CTM. Through the preserved atoms (C, S and reduced and oxidized N) the contributions of the separate sources are tracked for chemically active tracers. In addition to the determination of the concentration change, the contribution of each labelled category to each tracer is tracked in each process description. The categories can be configured flexibly, for instance by regions, sectors, or combinations thereof. For a detailed description of the source attribution used in the LOTOS-EUROS CTM we refer to Kranenburg et al. (2013). Applications to particulate matter and its precursor can be found in previous studies (Timmermans et al., 2017; Hendriks et al., 2016; Banzhaf et al., 2015; Curier et al., 2014; Schaap et al., 2013). In this study we focus on the source attribution of background concentrations of nitrogen oxides in terms of source sectors. To compare the source attribution methodologies, we used a limited set of 5 labels including the 4 main source sectors and the remaining other sectors combined. Table 1 contains detailed information on the available emission sources and the associated labels used in this study. The labelling system requires to label all sources of nitrogen oxides within the domain and therefore for the contribution of natural sources and boundary conditions were tracked as well.

An alternative method used for deriving source attribution information is provided by the brute force technique. We make use of the terminology of contributions and potential impacts  $PI_{S,X}$  as introduced by Thunis et al. (2020) to distinguish between the applied methods for source attribution. The brute force technique determines the impact  $I_{S,X}$  of a emission reduction in source sector  $S$  in comparison to a baseline

**Table 1**  
Source categories considered in this study.

Source Category	Source Composition
Road Transport	Gasoline, diesel, and LPG/gas powered light and heavy-duty vehicles, motorcycles, mopeds.
Non-Road Transport	Mobile sources excluding road-traffic such as aviation, rail, shipping, inland waterways and mobile machinery from agriculture and manufacturing industries.
Energy & Industries	Power plants for coal, liquid fuels, gas or solid biomass and associated combustion processes. Combustion in the industrial sector covering the production of iron and steel, pulp and paper or cement manufacturing as well as the chemical industry.
Households	Combustion processes of coal, gas, solid biomass, and liquid fuels of private households and small businesses.
Others	All other source sectors are combined into this category i.e., production processes for coal, oil, gas and flaring and emissions from the agricultural sector.

**Table 2**  
Overview of performed model simulations.

Simulation	Description of model set-up
BASE	Reference simulation without emission reduction and source attribution to compare with sensitivity simulations.
LA	Source attribution with labelled source sectors defined in Table 1 applying the labelling approach.
RED <sub>X</sub>	Emission sensitivity simulations performed individually for each source category (Table 1) according to the specific reduction level (X = 5, 10, 20, 25, 35, 50, 75, 100%) for NO <sub>x</sub> .
COMB <sub>X</sub>	Emission sensitivity simulations performed for all source categories simultaneously (Table 1) according to the specific reduction level (X = 5, 10, 20, 25, 35, 50, 75, 100%) for NO <sub>x</sub> .

concentration ( $I_{S,X} = \Delta C_{S,X} = C_{S,X} - C_{REF}$ ). When using a brute force approach, the selected emission source sectors and/or regions are reduced by a percentage  $X$ . Using a linearity assumption, the impact is converted into the potential impact  $PI_{S,X}$ , by scaling it to 100% by applying the multiplication factor  $100/X$  (Eq. 2). In this study we applied the brute force technique to NO<sub>x</sub> emissions using 8 reduction percentages ranging from  $X = 5, \dots, 100\%$  (hereafter indicated as **RED<sub>5</sub>**, ..., **RED<sub>100</sub>**). All reduction percentages were applied to each of the 5 source categories to investigate the sensitivity to the size of the emission reduction applied (Table 2). Furthermore, a set of sensitivity simulations were performed, in which emissions of all source sectors were reduced simultaneously to investigate additivity. We will use the term combined simulations when further referring to these scenarios (**COMB<sub>5</sub>**, ..., **COMB<sub>100</sub>**). Sensitivity simulations with individually reduced emission sectors are just referred to as sector reduction simulations. All in all, the number of annual simulations totals 49 on both domains: the baseline, 40 **RED<sub>X</sub>** and 8 **COMB<sub>X</sub>** simulations.

Eq. 2 Potential Impact

$$PI_{S,X} = \left| I_{S,X} \cdot \frac{100}{X} \right| \quad (2)$$

### 2.3. Metrics to evaluate the source attribution

To evaluate the source attribution for nitrogen oxides (NO<sub>2</sub>, NO and NO<sub>x</sub>), the labelled contributions and potential impacts were compared to each other by quantifying absolute and relative differences. NO<sub>x</sub> concentrations are provided in the mass equivalent of NO<sub>2</sub>. In addition, a linear regression model is used to compare the labelled contributions with potential impacts for each individual source sector. As statistical indicator, we calculated the root mean squared error (RMSE, Eq. 3). Besides the evaluation of spatial distributions, the modelling results were sampled for the background sites of the German monitoring network (UBA; [www.uba.de](http://www.uba.de)). We chose to select the monitoring sites with a 99% data availability. In total, 235 observation sites were included (Fig. 1). All monitoring sites were further clustered into their sub-categories of urban- (94), suburban- (66) and rural-background (75) stations. The site classification is used as an indicator to discriminate between more and less polluted areas in Germany. Observations at traffic and industrial locations were neglected as we are focusing on the background concentrations and as the resolution of chemistry transport models are not representative for conditions close to large sources.

To allow for a deeper insight and to diagnose the behavior of the brute force methodology, we deduce the degree of the non-linearity using the sensitivity simulations as suggested by Thunis et al. (2019). For non-linear systems a 10% emission reduction may yield a smaller or larger relative impact in the pollutant concentration. Moreover, a subsequent 10% reduction may not have the same impact as the first 10% reduction. Hence, the potential impacts for a sector may vary with the emission reduction percentage applied. In a linear regime they would be equal. Furthermore, the sum of the potential impacts of all sectors may not correspond to the modelled concentration in the baseline simulation. A proportionality analysis has been carried out to assess the degree of non-linearity in the responses to the emission reductions. Here, we defined an indicator based on the ratio between the impact  $I_{S,X}$  / potential impact  $PI_{S,X}$  of a given reduction level  $X$  (**RED<sub>X</sub>**) and the impact

$I_{S,20}$  / potential impact  $PI_{S,20}$  of the 20% reduction scenario (**RED<sub>20</sub>**), hereafter referred to as the consistency ratio for impacts **CRIS<sub>X</sub>** and potential impacts **CRPI<sub>S,X</sub>** (Eq. 4). By this, differences between individual reduction levels for impacts and potential impacts are highlighted. To illustrate, in an ideal case, the consistency ratio for the impact (**CRIS<sub>X</sub>**) of a linear/proportional relation would result in **CRIS<sub>X</sub> = X/20**. The consistency ratio for potential impacts (**CRPI**) would be equal to 1 for each reduction level. We decided to define a 20% reduction level to be used as reference criterion here, to be in line with the EMEP (European Monitoring and Evaluation Programme) and SHERPA (Screening for High Emission Reduction Potentials on Air quality) approach where 15% and 20% emission scenarios are applied, respectively. Applying the consistency ratio one can easily indicate the linear response to different emission reductions. With a proportional behavior, a linear regime can be assumed, and the impacts would be scalable. When the response to the emission reduction would be lower/larger than  $X$ , the consistency ratio would yield in a less/more than proportional reduction with respect to the emission reduction of  $X$  and one cannot perform a linear scaling of the impacts.

In addition, we determined the additivity to provide further evidence of non-linear responses (Thunis et al., 2019). The concentration derived by accumulating all potential impacts  $PI_{S,X}$  of the sector reduction simulations for a given reduction level  $X$  we refer to as the Sector Explained Mass **SEM<sub>X</sub>** (Eq. 5). The potential impact derived from the combined simulations (**COMB<sub>X</sub>**) are referred to as the Combined Explained Mass **CEM<sub>X</sub>**. By comparing the **SEM<sub>X</sub>** and the **CEM<sub>X</sub>** you proof additivity. Additivity is assured when the **SEM<sub>X</sub>** equals the **CEM<sub>X</sub>**. Inconsistencies that become present in this context are defined as lack of additivity. In that case, the Sector Explained Mass will not reflect the total mass of the baseline simulation (Thunis et al., 2020). We also introduced the acronym of the Labelled Explained Mass **LEM**, which is defined as the accumulated sum of all source sector contributions derived by the labelling simulation. The **LEM** is used when comparing the results side-by-side with respect to the **SEM<sub>X</sub>**.

Eq. 3 Root Mean Squared Error (RMSE)

$$RMSE_{S,X} = \sqrt{\frac{1}{N} \sum_{i=1}^N (PI_{S,X} - LA_S)^2} \quad (3)$$

Eq. 4 Consistency Ratio for Impact and Potential Impact

$$CRIS_X = \frac{I_{S,X}}{I_{S,20}}, \quad CRPI_{S,X} = \frac{PI_{S,X}}{PI_{S,20}} \quad (4)$$

Eq. 5 Sector Explained Mass

$$SEM_X = \sum_S PI_X \quad (5)$$

## 3. Results

### 3.1. Source attribution using the labelling approach

In this section, we present the sectoral source attribution of background concentrations for nitrogen oxides across Germany obtained using the labelling approach. In Germany, the largest emissions and associated concentrations for nitrogen oxides are found in major

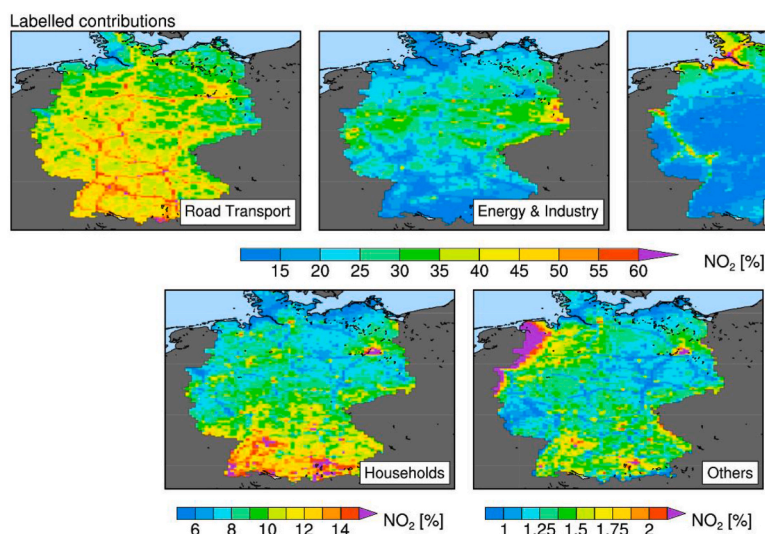


**Fig. 2.** Source attribution by the labelling approach (LA) across Germany for January to December 2018 shown as yearly average. Contributions of NO<sub>2</sub> are shown as relative share with respect to the absolute baseline concentration. (For interpretation of the references to color in this figure legend, the reader is referred to the Web version of this article.)

transportation corridors, industrialized areas (e.g. the Ruhr region) and urbanized agglomerations (e.g. Berlin, Munich, Hamburg) as shown in Fig. 2 & Fig. 4. Annual mean (urban) background concentration above 20 µg/m<sup>3</sup> are only modelled for these large cities. Under normal conditions, the emitted NO is readily converted to NO<sub>2</sub> explaining that most of the NO<sub>x</sub> is present in the form of NO<sub>2</sub>. For the buildup of NO first all ozone needs to be reacted away. Hence, the enhanced levels of NO are more clearly related to the areas with the largest emissions of nitrogen oxides i.e. the largest cities and transport corridors.

The concentration patterns for NO<sub>2</sub> can be further explained using the source attribution as provided in Fig. 2. The largest absolute and relative shares for road transport are modelled in the urban background of cities and along the highway network. The larger relative share in rural background in southern Germany as compared to northern Germany is explained by the absence of large emissions from industry and other transportation modes. The non-road transport contributions maximize in the Rhine Valley, the coastal regions and around the Kiel-Hamburg channel and are mainly explained by shipping emissions. Agricultural emissions (incorporated in others) contribute most to the total concentration in rural areas in northern Germany and near to the German Alps. Also, the relative contribution of households shows a striking gradient between northern and southern Germany. This can be explained with the spatial allocation for emissions across Germany. The accessibility to wood and number of (wood) stoves in southern parts of the country is larger than in the north. The larger emission density causes the north/south gradient. Although the absolute contribution of the industry and energy sector is largest in the Ruhr area, the relative contribution from this sector is notably larger in central and especially eastern Germany. The latter is explained by a number of larger power plants and industrial sites in this sparsely populated region.

In Fig. 3 the time series of modelled daily mean background concentrations and their sector contributions for 2018 are shown for NO<sub>x</sub>, NO<sub>2</sub> and NO. The time series represent the average across all rural, suburban, and urban background observation sites (depicted in Fig. 1) and show a seasonal cycle with larger concentrations in winter than in summer due to less favorable mixing conditions and larger anthropogenic emissions in winter. The amplitude of the seasonal variability is largest for nitrogen monoxide, as a buildup of NO occurs normally under conditions with shallow boundary layers, stagnant weather, and low background ozone levels.

As expected, the largest contributions are calculated for road transport followed by non-road transport, energy & industry, households, and

the smallest contribution for other emission source sectors (Fig. 3). For Fig. 3 and all statistics presented below the average across all background observation sites distinguishing their station type was used. In the urban background, relative contributions from road transport (URBG: 45 ± 5%, RUBG: 42 ± 5%) and households (URBG: 10 ± 6%, RUBG: 9 ± 5%) are on average slightly larger compared to those in rural background areas, while in rural background areas contributions from energy & industrial sources (URBG: 20 ± 3%, RUBG: 23 ± 4%) and non-road transport (URBG: 24 ± 6%, RUBG: 25 ± 7%) are slightly more pronounced (Fig. 2 & see App. 1). Contributions from households (DJF: 16 ± 4%, JJA: 4 ± 1%) as well as of energy & industry (DJF: 24 ± 3%, JJA: 19 ± 2%) show maximum values in winter, which can be related to additional energy demand and subsequent combustion emissions during the heating period (Fig. 3 & see App. 1).

### 3.2. Comparison of the 5-sector total attributed background concentration

We illustrate the behavior of source attribution results from the brute force simulations using the RED<sub>20</sub> scenarios. Fig. 4 shows the spatial distribution of the summed potential impact of all five sectors, the SEM<sub>20</sub>, in comparison to the labelling result. The absolute and relative differences in the annual average are shown in Fig. 5. The SEM<sub>20</sub> for NO shows large systematic deviations to the labelled source attribution results. The attributed total NO background concentration is tens of percent larger than with the labelling, showing largest deviations in the source regions. Both absolute and relative differences increase with shorter distance to the urban background. On annual average, the overestimation is about 53 ± 24% for urban and 40 ± 26% for rural background sites, respectively (see App. 2). Note that the attributed SEM<sub>20</sub> also largely overestimates the station averaged total modelled NO background concentration of the baseline by about 46 ± 25% (see App. 2). Relative deviations for NO<sub>2</sub> and NO<sub>x</sub> are considerably smaller than for NO (see App. 3 & App. 4). The SEM<sub>20</sub> of NO<sub>2</sub> is lower than attributed concentrations of the labelling in urban background areas (−3 ± 5%), with largest deviations in the cities along the Rhine and Main. In the rural background the difference changes sign systematic, indicating that the SEM<sub>20</sub> attributes a (4 ± 6%) larger concentration than the labelling approach. For NO<sub>x</sub> the differences are positive everywhere, with up to 6 ± 5% on station average. In the urban background, the relative difference is closer to zero which was expected as NO<sub>x</sub> is not as sensitive to the titration regimes as its constituents (see App. 4).

In Fig. 6 the time series for the SEM<sub>20</sub> minus the LEM are provided,

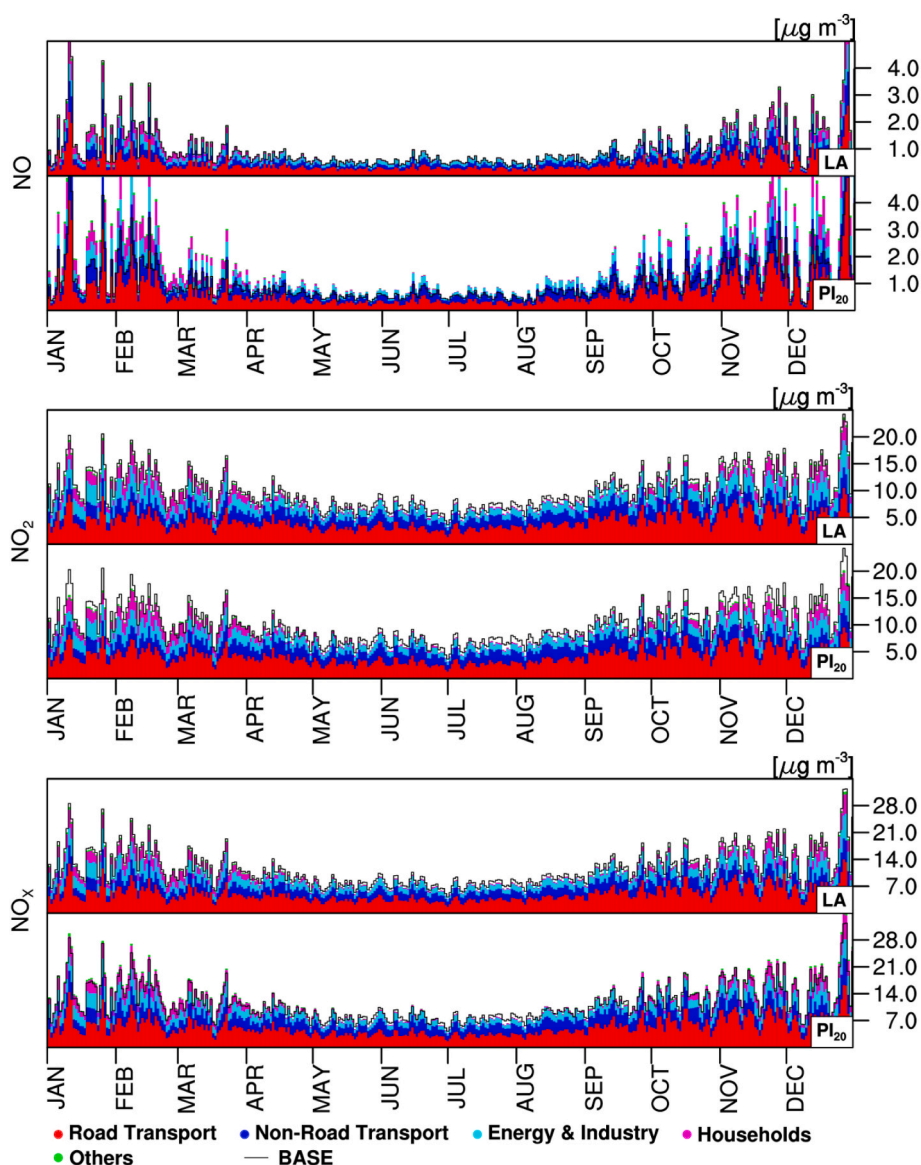


**Fig. 3.** Labelled contributions (LA) and potential impacts of a 20% NO<sub>x</sub> reduction (PI<sub>20</sub>) across Germany for January to December 2018 shown as daily average. Contributions and potential impacts of NO (top), NO<sub>2</sub> (center) and NO<sub>x</sub> (bottom) have been averaged over space across all German observation types. (For interpretation of the references to color in this figure legend, the reader is referred to the Web version of this article.)

showing the average across all background observation sites. The levels of the station average themselves for the **SEM**<sub>20</sub> and **LEM** can be read from Fig. 3. Inspection of the daily time series learns that the **SEM**<sub>20</sub> for NO is equal or (substantially) larger than the **LEM** throughout the year. For monthly values, averaged over all station locations, the **SEM**<sub>20</sub> overestimates the NO concentration up to  $75 \pm 18\%$  (see App. 3). Deviations between the techniques are more prevalent in winter (DJF:  $69 \pm 26\%$ ) than during the summer season (JJA:  $31 \pm 16\%$ ). In contrast, the **SEM**<sub>20</sub> of NO<sub>2</sub> can be larger or smaller throughout the year compared to the labelling. The underestimation occurs during periods with stagnation and thus the highest NO<sub>2</sub> levels (see explanation and example below). As mentioned above, the results for NO<sub>x</sub> show mostly an overestimation in comparison to the labelling results. The absolute differences follow the seasonal cycle of NO<sub>x</sub> itself. Note that on average urban background stations show larger deviations than rural ones for all compounds (see App. 1 to 4).

The different behavior for NO and NO<sub>2</sub> concerning the deviations between **SEM** and **LEM** can be explained by the occurrence of ozone limiting titration conditions (Fig. 7). The oxidation of NO is normally not

limited during daytime. However, the ground level ozone background concentration decreases fast during stable conditions occurring when fresh NO titrates the ozone. When the ozone is fully removed, NO<sub>2</sub> levels will only increase further by primary NO<sub>2</sub>, whereas NO starts to build up due to continuing emissions. In Fig. 7 this process is illustrated for four days in January 2018. During the first hours of two days of stagnant conditions (see the planetary boundary layer height in Fig. 7) the ozone is titrated away, after which a build-up of both NO and NO<sub>2</sub> occurs. For NO the background concentrations increase from near zero to exceed those of NO<sub>2</sub> with concentrations above  $100 \mu\text{g/m}^3$  in the peak at the 11<sup>th</sup>. After the weather changes the situation turns back to instable, mixed conditions with near-zero NO levels. This feature occurs frequently in winter when a limited amount of ozone is available caused by lower photochemical production of ozone and shallow boundary layers. A too large **SEM**<sub>20</sub> with respect to the **LEM** and baseline for NO simply occurs as for each sensitivity simulation it has been assumed to start from 100% emissions in the brute force approach. When the system stays in the regime with zero ozone the reduction in NO<sub>2</sub> is limited to the direct emission. In contrast, the NO levels are lowered more than

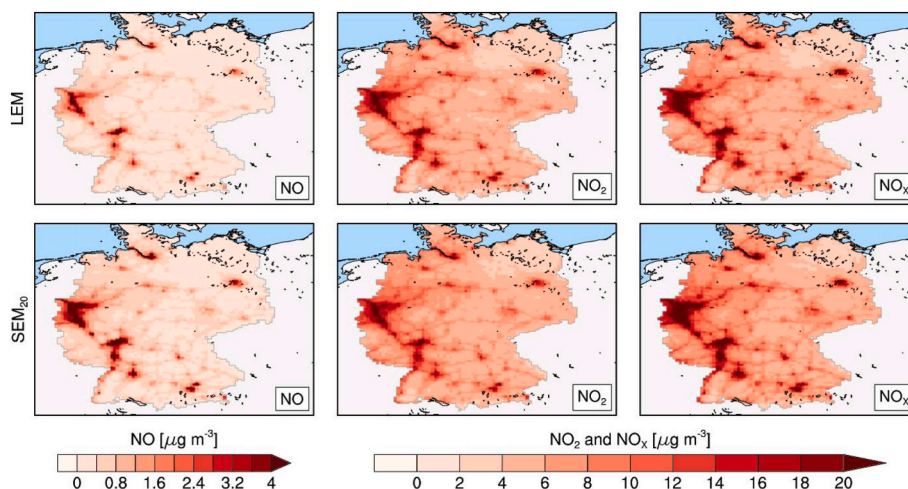


**Fig. 4.** Mass concentration of the Labelled Explained Mass (**LEM**, top) and Sector Explained Mass for the NO<sub>x</sub> reduction level of 20% (**SEM<sub>20</sub>**, bottom). From left to right: NO, NO<sub>2</sub> and NO<sub>x</sub>. (For interpretation of the references to color in this figure legend, the reader is referred to the Web version of this article.)

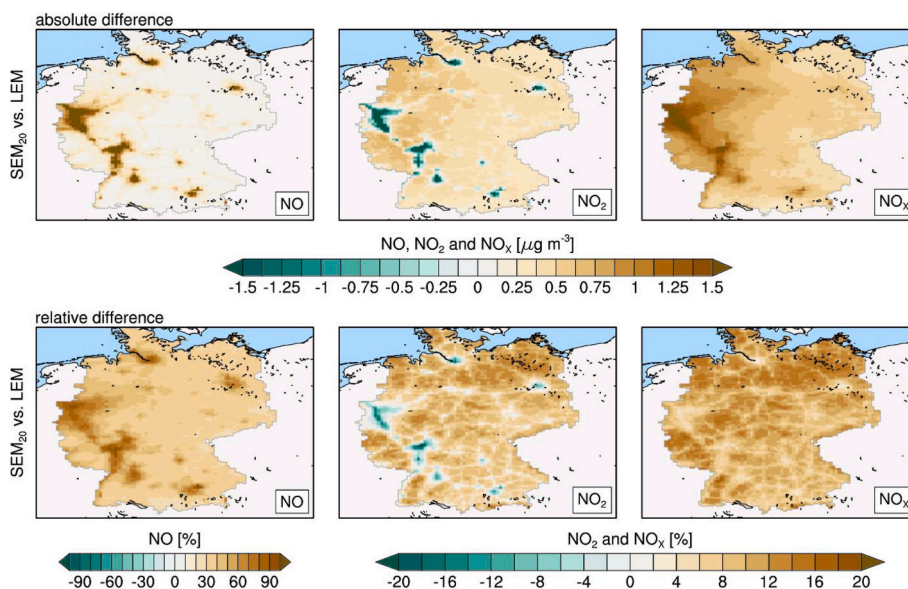


**Fig. 5.** Absolute (top) and relative (bottom) differences between Sector Explained Mass for NO<sub>x</sub> reduction level of 20% (**SEM<sub>20</sub>**) and the Labelled Explained Mass (**LEM**). From left to right: NO, NO<sub>2</sub> and NO<sub>x</sub>. (For interpretation of the references to color in this figure legend, the reader is referred to the Web version of this article.)

proportional to the NO<sub>x</sub> emission change (Fig. 7). Starting from the baseline for each reduction simulation means that this non-proportionality effect is incorporated in each individual brute force reduction simulation. With smaller NO<sub>x</sub> emission reductions, the likelihood of leaving the range where all ozone is completely titrated away is much smaller than for large emission reductions. Hence, the SEM<sub>x</sub> for NO will be larger when smaller reduction percentages are applied. During these conditions the reasoning for NO<sub>2</sub> is the other way around, whereas NO<sub>x</sub> in the source regions responds consistently with the emission reduction.

A further effect when applying reduction simulations is related to the lifetime of NO<sub>x</sub>. In the presence of NO during the night, the oxidation pathways of NO<sub>2</sub> to nitric acid do not take place. As it takes longer to titrate all ozone away with lowered NO<sub>x</sub> emissions, the duration in which this ozone limiting conditions are present is reduced in the reduction simulations. Hence, this allows ozone to oxidize NO<sub>2</sub> through heterogeneous chemistry and thus the lifetime of the NO<sub>2</sub> and NO<sub>x</sub> can be slightly reduced. This effect is more important in the less polluted

regions and leads to lower transport from source regions to more remote areas and thus a sign change for NO<sub>2</sub> in the rural areas.

### 3.3. Comparison of contributions and potential impacts for source sectors

In this section we compare the attribution to the individual sectors and add the dependency of the reduction percentage applied. Although the annual and monthly average share of NO<sub>2</sub> across the country is in close agreement for both methodologies (see App. 1 & App. 7), the deviations show spatial and temporal variability. Fig. 8 compares daily and hourly averages of potential impacts (PI<sub>x</sub>) with labelled contributions (LA) for all source sectors and for reduction fractions of X = 10, 20 and 75% using a regression analysis for NO<sub>2</sub>. From the comparison one sees that differences between potential impacts and labelled contributions are smaller for daily averaged values compared to hourly estimates. All source sectors show lower RMSE's for daily averaged values, when comparing the potential impacts with the labelled contributions. For example, the RMSE for road transport on an hourly basis is 0.52

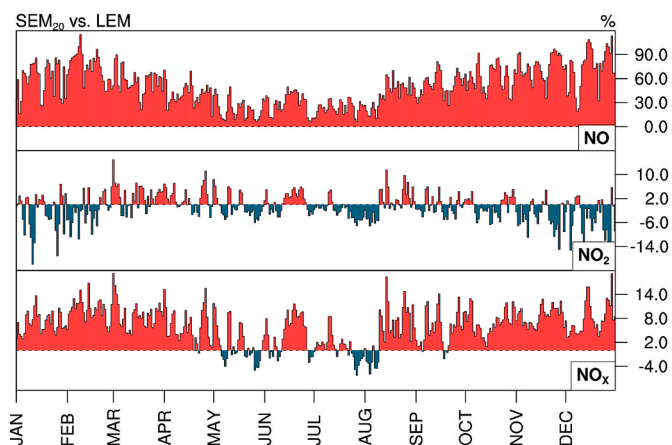


**Fig. 6.** Sector Explained Mass from NO<sub>x</sub> reduction level 20% (*SEM*<sub>20</sub>) minus the Labelled Explained Mass (*LEM*) across Germany for January to December 2018. The mass concentrations of NO (top), NO<sub>2</sub> (center) and NO<sub>x</sub> (bottom) have been averaged over all German background observation sites (rural, suburban, and urban). (For interpretation of the references to color in this figure legend, the reader is referred to the Web version of this article.)

compared to 0.24 on a daily basis for the 20% reduction scenario (see **App. 6**). Moreover, we notice a closer agreement between potential impacts and labelled contributions for the largest source sectors.

The spatial distribution for potential impacts and labelled contributions is compared in **Fig. 9** using annual averages. In **Fig. 9** the same source sectors and reduction levels are shown as used in **Fig. 8**. For road transport (URBG: 44 ± 5%, RUBG: 40 ± 5%), non-road transport (URBG: 25 ± 7, RUBG: 28 ± 8%), households (URBG: 10 ± 6%, RUBG: 9 ± 6%), and the remaining sources (URBG/RUBG: 1 ± 1%) the patterns follow the picture described for the *SEM*<sub>20</sub> above, with almost lower/larger potential impacts in urban/rural background areas compared to labelled contributions for NO<sub>2</sub> (see **App. 1 & App. 7**). The relative

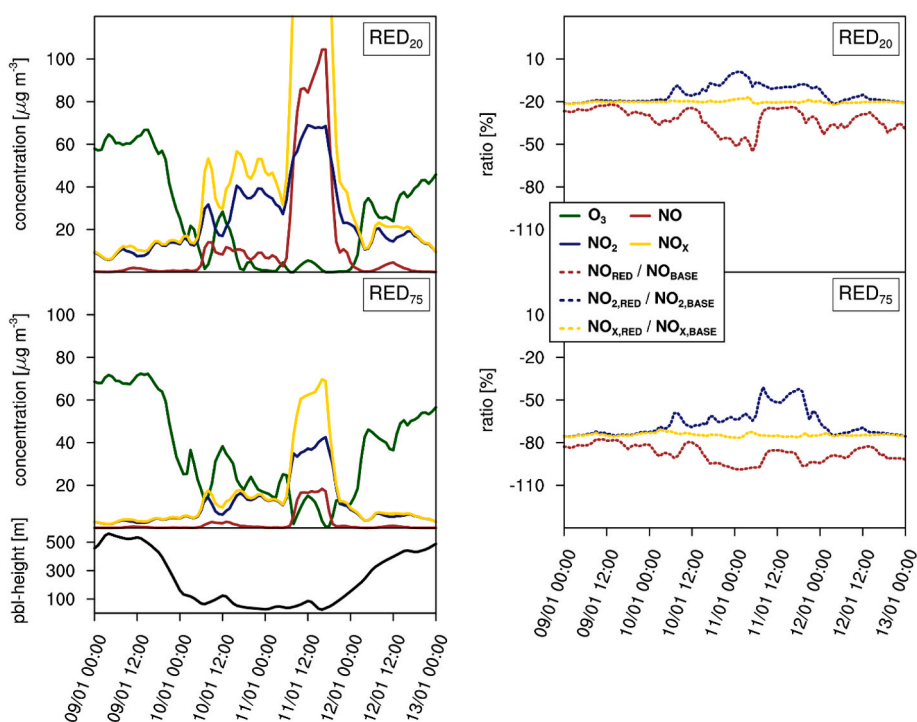


**Fig. 7.** Relation for NO, NO<sub>2</sub>, NO<sub>x</sub> and O<sub>3</sub> indicated for an urban background site in Berlin (capital of Germany) for 4 winter days in 2018. (For interpretation of the references to color in this figure legend, the reader is referred to the Web version of this article.)

difference for non-road transport is larger as a large fraction of the emissions is emitted during nighttime in comparison to the other sectors. The sector with a deviating behavior is the energy & industry sector (URBG: 18 ± 3%, RUBG: 22 ± 4%). Overall differences for small reduction fractions become larger for road transport, non-road transport and households, whereas differences for energy & industry increases with larger reduction fraction (**Figs. 8 and 9**). The different behavior of the power sector is attributed to the impact on ozone above the surface layer. This can be explained with contrasting interactions when emitting from the ground level or from high-stack sources. Emission reductions may enhance the ozone above the urban and industrialized areas which induces a small compensation effect through conversion of NO to NO<sub>2</sub> from the other sources when mixed towards the ground.

**Fig. 10** summarizes mentioned above findings for annual mean potential impacts (*PI*<sub>X</sub>) for all reduction levels as function of station categories and indicates that deviations between the *SEM*<sub>X</sub> and the *LEM* are sensitive to the chosen emission reduction fraction and increase for smaller reduction levels X. For example, the *SEM*<sub>5</sub> deviates on average -7 ± 5% from the baseline for NO<sub>2</sub> at urban background stations, whereas the relative difference for the *SEM*<sub>20</sub> is -8 ± 5%. The differences are smaller for rural background conditions where the *SEM*<sub>5</sub> deviates on average -3 ± 8%. The results for NO indicate a deviation of 54 ± 26% for *SEM*<sub>5</sub> in comparison to 48 ± 25% for *SEM*<sub>20</sub>. The differences between urban and rural background environments are related to the frequency of ozone limiting titration regimes as already described in section 3.2.

### 3.4. Non-linearity and additivity of the brute force results

In this section we illustrate the response to different emission reductions using the consistency ratio of impacts (*CRI*) and potential impacts (*CRPI*) as already introduced and explained in the methodology section. **Fig. 11** shows the *CRI* (left) and *CRPI* (right) for all emission reduction levels for NO (top), NO<sub>2</sub> (mid) and NO<sub>x</sub> (bottom). Here, a linear regime can be assumed when the *CRI* shows a proportional behavior. In that case, the impacts are scalable and the *CRPI* for each

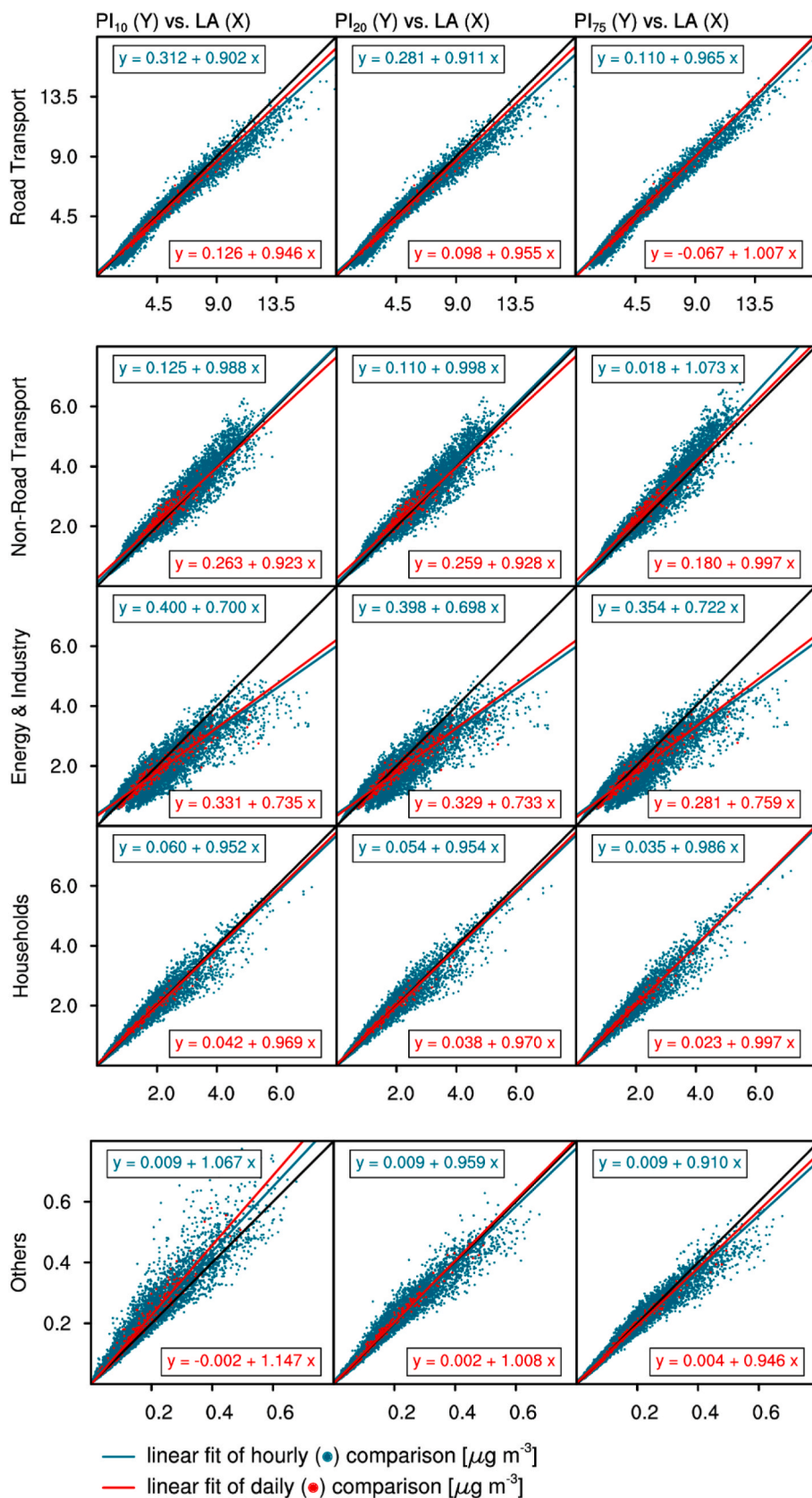


**Fig. 8.** Differences of potential impacts from NO<sub>x</sub> reduction levels 10, 20, and 75% ( $PI_{10}$ ,  $PI_{20}$ , and  $PI_{75}$ ; y-axis) compared to labelled contributions (LA; x-axis) across Germany for January to December 2018. The mass concentration of NO<sub>2</sub> has been averaged over space. (For interpretation of the references to color in this figure legend, the reader is referred to the Web version of this article.)

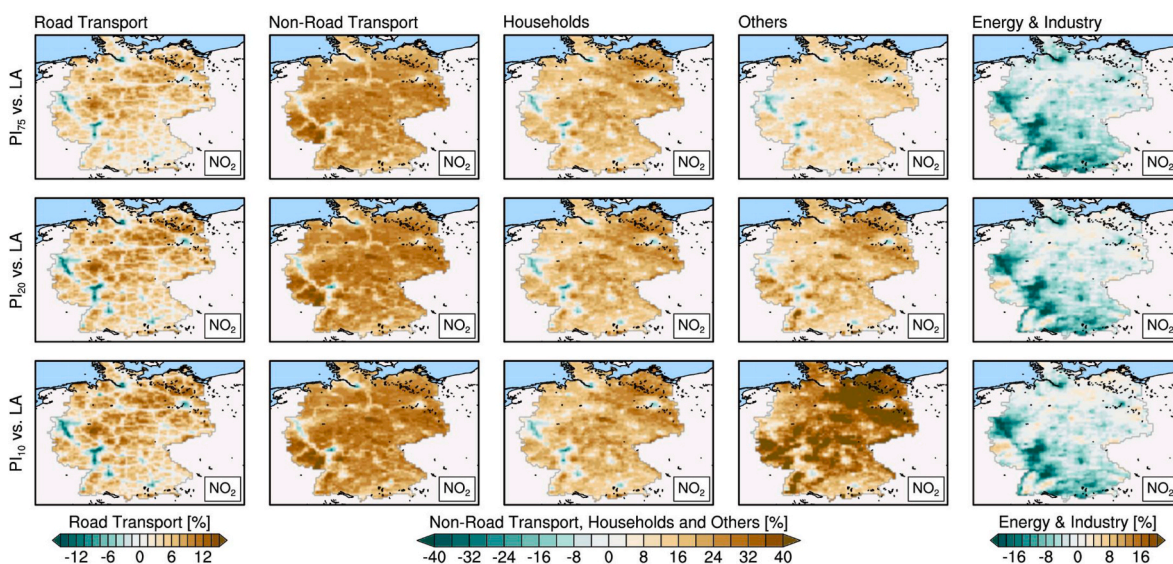


Fig. 9. Same as in Fig. 8 with relative differences and averaged in time. (For interpretation of the references to color in this figure legend, the reader is referred to the Web version of this article.)

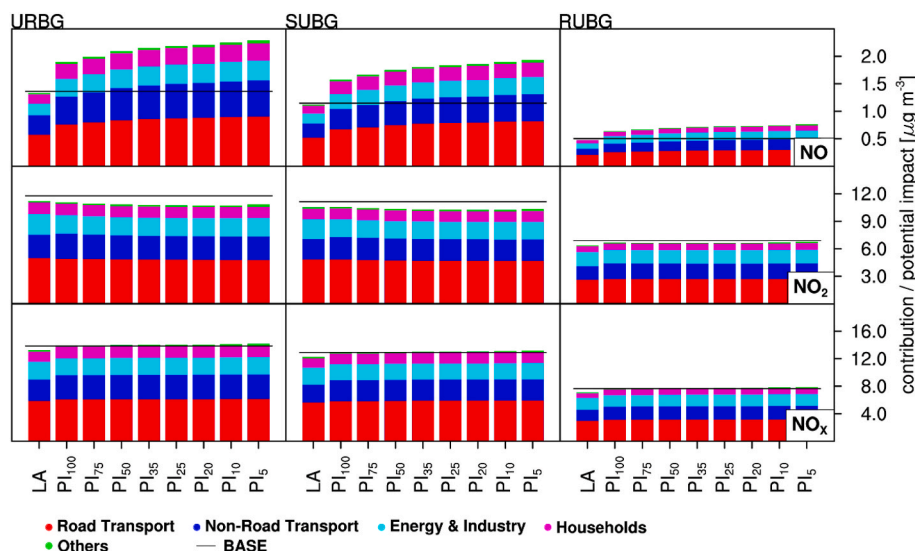


Fig. 10. Labelled contributions (LA) and potential impacts of NO<sub>x</sub> reduction levels from 5 to 100% (PI<sub>5</sub>, ..., PI<sub>100</sub>) across Germany for January to December 2018. Three station types have been investigated and are presented from left to right (urban background: URBG, sub-urban background: SUBG, and rural background: RUBG). The mass concentration of NO (top), NO<sub>2</sub> (center) and NO<sub>x</sub> (bottom) have been averaged over time and space. (For interpretation of the references to color in this figure legend, the reader is referred to the Web version of this article.)

emission reduction fraction would be 1. When the *CRI* shows a less or more than proportional reduction (with respect to the emission fraction of *X*), the linear scaling of the impacts differs from 1 for the *CRPI*.

The *CRI* indicates that reduced NO<sub>x</sub> emissions do not lead to a proportional reduction of the NO concentration amount for the German background (Fig. 11, top left). This indicates that NO<sub>x</sub> emission reductions of level *X* lead to a NO response larger than *X*. Largest differences to a proportional reduction can be seen for the combined reduction scenario and for the non-road transport source sector of about 35% and 20% respectively, which can be seen by the offset from the ideal case (*X*/20). The remaining source sectors (others) show the most linear relation with differences to the ideal case of about 1.5% as the regime change does hardly occur. The *CRI* for NO<sub>2</sub> and NO<sub>x</sub> shows an almost proportional behavior, as the errors for certain changes are small. For example, the difference to a proportional emission reduction between 5 and 50 percent is within 1.5% for both compounds and within 5% between 5 and 100 percent reduction. Overall, the proportionality of the *CRI* is reduced with higher emission reductions of NO<sub>x</sub> for all compounds.

The proportionality for consistency ratios of potential impacts *CRPI* are decreasing with higher reduction levels, similar to the *CRI* (Fig. 11, right) as shown by their offset to 1. When only considering the 4 main source sectors, the largest differences for NO are evident for non-road transport (20%) and lowest for households (9%). Even larger deviations are obvious for the combined reduction scenario (35%). For NO<sub>2</sub> and total NO<sub>x</sub>, the *CRPI* reveals an almost proportional behavior with differences within 2–5% each. By considering the *CRPI* for remaining sources (others), considerably larger differences can be seen for NO (43%), NO<sub>2</sub> (37%) and NO<sub>x</sub> (24%), respectively. This can be explained by the linear scaling to 100% to estimate the potential impact of each source sector and indicates that small-sized emission categories are related to larger differences due to increased non-linearities as they remain more often in the titration regime.

To further highlight the non-linear interaction of emission reductions to nitrogen oxides, we performed an additivity analysis. Fig. 12 shows the Sector Explained Mass (*SEM*, in black) and Combined Explained Mass (*CEM*, in red) of NO, NO<sub>2</sub> and total NO<sub>x</sub>. The results suggest that on average for NO<sub>2</sub> additivity is present within 2% (see App. 5). This

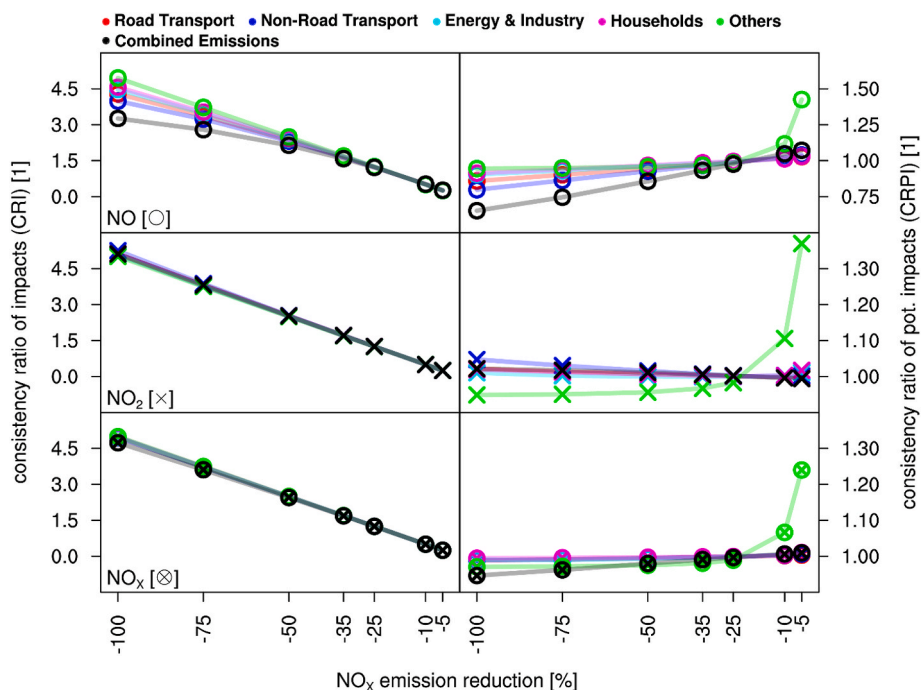


Fig. 11. Consistency ratios for impacts (left) and potential impacts (right) for NO (top), NO<sub>2</sub> (mid) and NO<sub>x</sub> (bottom). Sector and combined reduction simulations for 5 to 100% are divided by different colors. (For interpretation of the references to color in this figure legend, the reader is referred to the Web version of this article.)

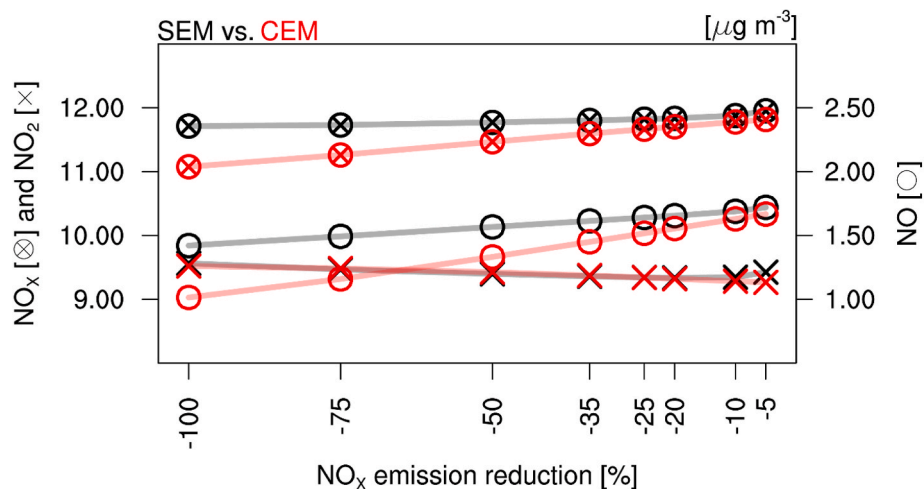


Fig. 12. Additive behavior of the source attribution for the brute force technique, of NO<sub>x</sub> reduction levels from 5 to 100%, across Germany for January to December 2018. Potential Impacts of combined emission reduction simulations (CEM) are shown in red, with potential impacts of added and individually reduced source sectors are represented in black (SEM). (For interpretation of the references to color in this figure legend, the reader is referred to the Web version of this article.)

correlate to the proportional concentration response to the NO<sub>x</sub> emission reduction, which was shown for NO<sub>2</sub>. A lack of additivity can be seen for NO, where the additivity is reduced with higher reduction levels. Here, additivity can only be assumed for reduction levels up to about -25%. For larger reduction percentages, differences of up to 40% can be seen between the SEM<sub>x</sub> and the CEM<sub>x</sub> (see App. 5). Reducing the emissions of a single sector by 50 or 100% implies one leaves the regime in several sector reduction simulations, which is not the case with small reductions. Hence, the emission reduction to leave the regime counted several times at large reduction percentages. In the combined reduction simulations, all NO<sub>x</sub> is removed and in the individual simulations only a part of total NO<sub>x</sub> is diminished. Based on this, in the combined simulations more impact of the overall chemistry change (e.g. NO<sub>x</sub>

dependent ozone formation in summer) can be seen as an additional effect. For NO<sub>x</sub>, the largest deviations between the SEM<sub>x</sub> and CEM<sub>x</sub> can be seen for higher reduction scenarios. However, as the averaged deviation between the SEM<sub>100</sub> and CEM<sub>100</sub> is overall small with about 5.8%, additivity can be assumed for NO<sub>x</sub> (see App. 5).

#### 4. Discussion and conclusion

In this study we compared the source attribution from the brute force and the labelling methods for nitrogen oxides. We successfully enhanced the understanding of limitations due to non-linearity triggered by the photochemical equilibrium of the Leighton cycle (Finlayson-Pitts and Pitts, 2000; Leighton, 1961). As summarized in previous studies, these

non-linear chemical processes are the main limiting factors for different source attribution approaches for different compounds. Our study advances these findings by adding a source attribution evaluation for background levels of nitrogen oxides. Lessons learned from this study might be beneficial to support the joint FAIRMODE (Forum for AIR quality Modelling) initiative for assessing the source attribution, developing strategies to explain the observed contributions in urban, suburban and rural background locations of nitrogen oxides as a first starting point for further mitigation purposes.

It is well known that NO levels are lowered more than proportionally with respect to NO<sub>x</sub> emission reductions. This is explained by the situation that NO levels build up under high NO<sub>x</sub> conditions when ozone has been removed by titration. Hence, a 10% reduction of NO<sub>x</sub> has a larger effect on NO than subsequent 10% reductions while the chemical regime is still ozone titrating. Whereas emission reduction simulations can explore the impacts of the emission change on NO levels, upscaling the impacts towards 100% (to estimate contributions) leads to systematically larger levels of attributed NO compared to the labelling approach. The resulting deviations between the explained mass of the brute force approach and the labelled results become larger when smaller emission reduction fractions are applied, which is in contrast to findings obtained from studies for particulate matter (Thunis et al., 2020, 2019; Carnevale et al., 2018; Clappier et al., 2017). Moreover, a source attribution for a single sector, based on emission reduction simulations and a baseline should be avoided as there is no way to verify for consistency and the approach will largely overestimate the sector explained mass. In the study we showed station-based differences on annual average, which vary about  $46 \pm 25\%$  from the baseline and a lack of additivity for NO of up to 40%. Thus, we conclude that the application of brute force simulations is potentially not the most suitable option for performing a source attribution in a consistent manner to estimate contributions of specific sources for NO.

Kwok et al. (2015) already indicates that the non-linear nature of ozone limits the applicability of potential impacts for NO<sub>2</sub>. We agree that the source attribution of NO and NO<sub>2</sub> is affected by the non-linear photochemical equilibrium for ozone and nitrogen oxides and therefore can be perturbed, especially during nocturnal winter periods. It should be noted that model simulations with low emission reduction levels (<25%) can be performed to reduce deviations caused by ozone-limiting conditions as additivity and linearity can be assumed to a certain degree. However, our study shows that larger deviations can be seen when small-sized emission source sectors are perturbed compared to large-sized sector categories. This implies that separating out more source sectors (and thus smaller sized ones), investigations may encounter larger problems due to the non-linearities induced by the titration regimes. This result is comparable to Belis et al. (2020), in which the authors indicate that the brute force technique fails to reflect the impact of varying emission levels in a specific source sector with related chemical reaction processes on any other sector. In addition, inconsistencies between the brute force technique and the baseline are increased in urban background regions, near emission sources. This is in agreement with Verstraeten et al. (2018), who emphasized that small-scale uncertainties become more relevant in urban areas, due to non-linear chemical phenomena. As these are the regions where limit values are exceeded and health effects are greatest, it is unfortunate that the inconsistency is most pronounced here. Still, since for NO<sub>2</sub> linearity and additivity can be assumed and the differences between potential impacts and labelled sector contributions are relatively small (<15%), the brute force technique is an appropriate method to be used to estimate the contributions of the main sectors for NO<sub>2</sub>. These differences are considerably smaller than typical systematic underestimations of CTMs to the observed ambient total NO<sub>2</sub> concentration, which can be in the order of a factor of 2 (e.g. Kuik et al., 2018; Schaap et al., 2015). However, when small-sized emission sectors are under investigation, we recommend avoiding the upscaling of sensitivity simulations for NO<sub>2</sub>.

The use of a labelling approach has several practical advantages as

the internal consistency is enforced by design and computational burden and chances of errors are lower (Kranenburg et al., 2013; Wagstrom et al., 2008). In addition, the flexibility for defining the labels is large, including the contributions of natural and boundary conditions (Carnevale et al., 2018). Comparative studies carried out by Thunis et al. (2019) and Clappier et al. (2017) indicate that the labelling approach may not always be an appropriate method to derive the impact of emission reduction options for mitigation purposes. They state that non-linear chemical mechanisms, in particular indirect processes, cannot be modelled and a linear scaling of the simulated mass or share for the source sectors cannot be performed for varying emission levels. In the same vein, the emission changes induced by mitigation options often differ substantially from the idealized reduction scenarios of the brute force method. Hence, explicit simulations of dedicated mitigation packages must be performed in any case.

For air quality planning, an initial quantification of the impact of emission reductions as well as the contribution for different source sectors are of decisive interest but each approach has its own limitation. Hence, we suggest combining both. We recommend conducting brute force sensitivity simulations based on the ranking of source contributions obtained from a labelling approach and to define this as the best practice for the air pollution management of nitrogen oxides for source attribution purposes. The studies by Mertens et al. (2018) and Butler et al. (2020) already indicate that for ozone, a combination of the perturbation and the tagging approaches can yield complementary information that neither approach can deliver on its own. As by definition combined simulations would be additive and able to represent indirect processes as well as the natural and boundary contribution could be separated out, this would widen the scope of advice to mitigate air-pollution. However further analysis is needed to gain a deeper understanding of the interactions of such combined concepts.

#### CRediT authorship contribution statement

**M. Thürkow:** Conceptualization, Methodology, Software, Validation, Formal analysis, Investigation, Resources, Data curation, Writing – original draft, Writing – review & editing, Visualization. **S. Banzhaf:** Writing – review & editing. **T. Butler:** Writing – review & editing. **J. Pültz:** Conceptualization, Methodology, Software, Resources, Writing – review & editing. **M. Schaap:** Conceptualization, Methodology, Writing – review & editing, Supervision, Project administration, Funding acquisition.

#### Declaration of competing interest

The authors declare that they have no known competing financial interests or personal relationships that could have appeared to influence the work reported in this paper.

#### Data availability

Data will be made available on request.

#### Acknowledgements

This research was funded by the Federal Ministry of Transport and Digital Infrastructure (BMVI) within the framework of the mFUND research initiative (grant no. 19F2065). The authors would like to thank the HPC Service of ZEDAT, Freie Universität Berlin, for computing time (Bennett et al., 2020).

#### Appendix A. Supplementary data

Supplementary data to this article can be found online at <https://doi.org/10.1016/j.atmosenv.2022.119412>.

## References

- Amann, M., Bertok, I., Borken-Kleefeld, J., Cofala, J., Heyes, C., Höglund-Isaksson, L., Klimont, Z., Nguyen, B., Posch, M., Rafaj, P., Sandler, R., Schöpp, W., Wagner, F., Winar, W., 2011. Cost-effective control of air quality and greenhouse gases in Europe: modeling and policy applications. *Environ. Model. Software* 26, 1489–1501. <https://doi.org/10.1016/j.envsoft.2011.07.012>.
- Banzhaf, S., Schaap, M., Kerschbaumer, A., Reimer, E., Stern, R., Van Der Swaluw, E., Builjtes, P., 2012. Implementation and evaluation of pH-dependent cloud chemistry and wet deposition in the chemical transport model REM-Calgrid. *Atmos. Environ.* <https://doi.org/10.1016/j.atmosenv.2011.10.069>.
- Banzhaf, S., Schaap, M., Kranenburg, R., Manders, A.M.M., Segers, A.J., Visschedijk, A.J.H., Denier van der Gon, H.A.C., Kuenen, J.J.P., van Meijgaard, E., van Ulft, L.H., Cofala, J., Builjtes, P.J.H., 2015. Dynamic model evaluation for secondary inorganic aerosol and its precursors over Europe between 1990 and 2009. *Geosci. Model Dev. (GMD)* 8, 1047–1070. <https://doi.org/10.5194/gmd-8-1047-2015>.
- Beelen, R., Raaschou-Nielsen, O., Stafoggia, M., Andersen, Z.J., Weinmayr, G., Hoffmann, B., Wolf, K., Samoli, E., Fischer, P., Nieuwenhuijsen, M., Vineis, P., Xun, W.W., Katsouyanni, K., Dimakopoulou, K., Oudin, A., Forsberg, B., Modig, L., Havulinna, A.S., Lanki, T., Turunen, A., Oftedal, B., Nystad, W., Nafstad, P., De Faire, U., Pedersen, N.L., Östenson, C.-G., Fratiglioni, L., Penell, J., Korek, M., Pershagen, G., Eriksen, K.T., Overvad, K., Ellermann, T., Eeftens, M., Peeters, P.H., Meliefste, K., Wang, M., Bueno-de-Mesquita, B., Sugiri, D., Krämer, U., Heinrich, J., de Hoogh, K., Key, T., Peters, A., Hampel, R., Concin, H., Nagel, G., Ineichen, A., Schaffner, E., Probst-Hensch, N., Künzli, N., Schindler, C., Schikowski, T., Adam, M., Phuleria, H., Villier, A., Clavel-Chapelon, F., Declercq, C., Grioni, S., Krogh, V., Tsai, M.-Y., Ricceri, F., Sacerdote, C., Galassi, C., Migliore, E., Ranzi, A., Cesaroni, G., Badaloni, C., Forastiere, F., Tamayo, I., Amiano, P., Dorronsoro, M., Katsoulis, M., Trichopoulos, A., Brunekreef, B., Hoek, G., 2014. Effects of long-term exposure to air pollution on natural-cause mortality: an analysis of 22 European cohorts within the multicentre ESCAPE project. *Lancet* 383, 785–795. [https://doi.org/10.1016/S0140-6736\(13\)62158-3](https://doi.org/10.1016/S0140-6736(13)62158-3).
- Belis, C.A., Pernigotti, D., Pirovano, G., Favez, O., Jaffrezou, J.L., Kuenen, J., Denier van der Gon, H., Reizer, M., Riffault, V., Alleman, L.Y., Almeida, M., Amato, F., Angyal, A., Argyropoulos, G., Bände, S., Beslic, I., Besombes, J.-L., Bove, M.C., Broto, P., Calori, G., Cesari, D., Colombi, C., Contini, D., De Gennaro, G., Di Gilio, A., Diapoulis, E., El Haddad, I., Elbern, H., Eleftheriadis, K., Ferreira, J., Vivanco, M.G., Gilardoni, S., Golly, B., Hellebust, S., Hopke, P.K., Izadmanesh, Y., Jorquera, H., Krajsek, K., Kranenburg, R., Lazzeri, P., Lenartz, F., Lucarelli, F., Maciejewska, K., Manders, A., Manousakas, M., Masiol, M., Mircea, M., Mooibroek, D., Nava, S., Oliveira, D., Paglione, M., Pandolfi, M., Perrone, M., Petralia, E., Pietrodangelo, A., Pillion, S., Pokorna, P., Prati, P., Salameh, D., Samara, C., Samek, L., Saraga, D., Sauvage, S., Schaap, M., Scotto, F., Segal, K., Siour, G., Tauler, R., Valli, G., Vecchi, R., Venturini, E., Vestenius, M., Waked, A., Yubero, E., 2020. Evaluation of receptor and chemical transport models for PM10 source apportionment. *Atmos. Environ.* X 5, 100053. <https://doi.org/10.1016/J.AEAOA.2019.100053>.
- Bennett, L., Melchers, B., Propp, B., 2020. *Curta: A General-Purpose High-Performance Computer at ZEDAT. Freie Universität Berlin*.
- Butler, T., Lupascu, A., Coates, J., Zhu, S., 2018. Toast 1.0: tropospheric ozone attribution of sources with tagging for CEM5 1.2.2. *Geosci. Model Dev. (GMD)* 11. <https://doi.org/10.5194/gmd-11-2825-2018>.
- Butler, T., Lupascu, A., Nalam, A., 2020. Attribution of ground-level ozone to anthropogenic and natural sources of nitrogen oxides and reactive carbon in a global chemical transport model. *Atmos. Chem. Phys.* 20 <https://doi.org/10.5194/acp-20-10707-2020>.
- Carnevale, C., Angelis, E. De, Finzi, G., Pederzoli, A., Turrini, E., Volta, M., 2018. A non linear model approach to define priority for air quality control. *IFAC-PapersOnLine* 51, 210–215. <https://doi.org/10.1016/j.ifacol.2018.07.280>.
- Clappier, A., Belis, C.A., Pernigotti, D., Thunis, P., 2017. Source apportionment and sensitivity analysis: two methodologies with two different purposes. *Geosci. Model Dev. (GMD)*. <https://doi.org/10.5194/gmd-10-4245-2017>.
- Curier, R.L., Kranenburg, R., Segers, A.J.S., Timmermans, R.M.A., Schaap, M., 2014. Synergistic use of OMI NO2 tropospheric columns and LOTOS-EUROPS to evaluate the NOx emission trends across Europe. *Remote Sens. Environ.* 149, 58–69. <https://doi.org/10.1016/j.rse.2014.03.032>.
- EEA, 2018. Air quality in Europe - 2018 report. European Environment Agency (EEA). Report No 12. Retrieved from: <https://www.eea.europa.eu/publications/air-quality-in-europe-2018>.
- European Parliament; European Council, 2008. Directive 2008/50/EC on ambient air quality and cleaner air for Europe. *Off. J. Eur. Communities* 152, 1–43. <http://eur-lex.europa.eu/LexUriServ/LexUriServ.do?uri=OJ:L:2008:152:0001:0044:EN:PDF>.
- Finlayson-Pitts, B.J., Pitts, J.N., 2000. Global tropospheric chemistry and climate change. In: *Chemistry of the Upper and Lower Atmosphere*, pp. 762–843. <https://doi.org/10.1016/B978-012257060-5/50016-2>.
- Fischer, P.H., Marra, M., Ameling, C.B., Hoek, G., Beelen, R., de Hoogh, K., Breugelmanns, O., Kruize, H., Janssen, N.A.H., Houthuijs, D., 2015. Air pollution and mortality in seven million adults: the Dutch environmental longitudinal study (DUELS). *Environ. Health Perspect.* 123, 697–704. <https://doi.org/10.1289/ehp.1408254>.
- Flemming, J., Inness, A., Flentje, H., Huijnen, V., Moinat, P., Schultz, M.G., Stein, O., 2009. Coupling global chemistry transport models to ECMWF's integrated forecast system. *Geosci. Model Dev. (GMD)* 2, 253–265. <https://doi.org/10.5194/gmd-2-253-2009>.
- Fountoukis, C., Nenes, A., 2007. Isorropia II: a computationally efficient thermodynamic equilibrium model for  $K^+$ - $Ca^{2+}$ - $Mg^{2+}$ - $NH_4^+$ - $Na^+$ - $SO_4^{2-}$ - $NO_3$ . *Atmos. Chem. Phys.* 7, 4639–4659.
- Fowler, D., Coyle, M., Skiba, U., Sutton, M.A., Cape, J.N., Reis, S., Sheppard, L.J., Jenkinson, A., Grizzetti, B., Galloway, J.N., Vitousek, P., Leach, A., Bouwman, A.F., Butterbach-Bahl, K., Dentener, F., Stevenson, D., Amann, M., Voss, M., 2013. The global nitrogen cycle in the twenty-first century. *Philos. Trans. R. Soc. B Biol. Sci.* 368 <https://doi.org/10.1098/rstb.2013.0164>.
- Granier, C., Bessagnet, B., Bond, T., D'Angiola, A., Denier van der Gon, H., Frost, G.J., Heil, A., Kaiser, J.W., Kinne, S., Klimont, Z., Kloster, S., Lamarque, J.-F., Liousse, C., Masui, T., Meuleux, F., Mieville, A., Ohara, T., Raut, J.-C., Riahi, K., Schultz, M.G., Smith, S.J., Thompson, A., van Aardenne, J., van der Werf, G.R., van Vuuren, D.P., 2011. Evolution of anthropogenic and biomass burning emissions of air pollutants at global and regional scales during the 1980–2010 period. *Clim. Change* 109, 163–190. <https://doi.org/10.1007/s10584-011-0154-1>.
- Hendriks, C., Kranenburg, R., Kuenen, J., van Gijlswijk, R., Wichink Kruit, R., Segers, A., Denier van der Gon, H., Schaap, M., 2013. The origin of ambient particulate matter concentrations in The Netherlands. *Atmos. Environ.* <https://doi.org/10.1016/j.atmosenv.2012.12.017>.
- Hendriks, C., Kranenburg, R., Kuenen, J.J.P., Van den Bril, B., Verguts, V., Schaap, M., 2016. Ammonia emission time profiles based on manure transport data improve ammonia modelling across north western Europe. *Atmos. Environ.* 131, 83–96. <https://doi.org/10.1016/J.ATMOSENV.2016.01.043>.
- Huang, Y., Deng, T., Li, Z., Wang, N., Yin, C., Wang, S., Fan, S., 2018. Numerical simulations for the sources apportionment and control strategies of PM2.5 over Pearl River Delta, China, part I: inventory and PM2.5 sources apportionment. *Sci. Total Environ.* 634, 1631–1644. <https://doi.org/10.1016/j.scitotenv.2018.04.208>.
- Kaiser, J.W., Heil, A., Andreae, M.O., Benedetti, A., Chubarova, N., Jones, L., Morcrette, J.-J., Razinger, M., Schultz, M.G., Suttie, M., van der Werf, G.R., 2012. Biomass burning emissions estimated with a global fire assimilation system based on observed fire radiative power. *Biogeosciences* 9, 527–554. <https://doi.org/10.5194/bg-9-527-2012>.
- Kampa, M., Castanas, E., 2008. Human health effects of air pollution. *Environ. Pollut.* 151, 362–367. <https://doi.org/10.1016/j.envpol.2007.06.012>.
- Kimbrough, S., Chris Owen, R., Snyder, M., Richmond-Bryant, J., 2017. NO to NO2 conversion rate analysis and implications for dispersion model chemistry methods using Las Vegas, Nevada near-road field measurements. *Atmos. Environ.* 165, 23–34. <https://doi.org/10.1016/j.atmosenv.2017.06.027>.
- Koo, B., Wilson, G.M., Morris, R.E., Dunker, A.M., Yarwood, G., 2009. Comparison of source apportionment and sensitivity analysis in a particulate matter air quality model. *Environ. Sci. Technol.* 43, 6669–6675. <https://doi.org/10.1021/es9008129>.
- Kranenburg, R., Segers, A.J., Hendriks, C., Schaap, M., 2013. Source apportionment using LOTOS-EUROPS: module description and evaluation. *Geosci. Model Dev. (GMD)* 6, 721–733. <https://doi.org/10.5194/gmd-6-721-2013>.
- Kuik, F., Kerschbaumer, A., Lauer, A., Lupascu, A., Von Schneidmesser, E., Butler, T.M., 2018. Top-down quantification of NOx emissions from traffic in an urban area using a high-resolution regional atmospheric chemistry model. *Atmos. Chem. Phys.* 18 <https://doi.org/10.5194/acp-18-8203-2018>.
- Kwok, R.H.F., Baker, K.R., Napelenok, S.L., Tonnesen, G.S., 2015. Photochemical grid model implementation and application of VOC, NO<sub>x</sub> and O<sub>3</sub> source apportionment. *Geosci. Model Dev.* 8, 99–114. <https://doi.org/10.5194/gmd-8-99-2015>.
- Leighton, P., 1961. *Photochemistry of Air Pollution*, first ed. Academic Press, New York.
- Lim, S.S., Vos, T., Flaxman, A.D., Danaei, G., Shibuya, K., Adair-Rohani, H., Amann, N., Anderson, H.R., Andrews, K.G., Aryee, M., Atkinson, C., Bacchus, L.J., Bahalim, A.N., Balakrishnan, K., Balmes, J., Barker-Collo, S., Baxter, A., Bell, M.L., Blore, J.D., Blyth, F., Bonner, C., Borges, G., Bourne, R., Boussinesq, M., Brauer, M., Brooks, P., Bruce, N.G., Brunekreef, B., Bryan-Hancock, C., Bucello, C., Buchbinder, R., Bull, F., Burnett, R.T., Byers, T.E., Calabria, B., Carapetis, J., Carnahan, E., Chafe, Z., Charlson, F., Chen, H., Chen, J.S., Cheng, A.T.A., Child, J.C., Cohen, A., Colson, K.E., Cowie, B.C., Darby, S., Darling, S., Davis, A., Degenhardt, L., Dentener, F., Des Jarlais, D.C., Devries, K., Dherani, M., Ding, E.L., Dorsey, E.R., Driscoll, T., Edmond, K., Ali, S.E., Engell, R.E., Erwin, P.J., Fahimi, S., Falder, G., Farzadfar, F., Ferrari, A., Finucane, M.M., Flaxman, S., Fowkes, F.G.R., Freedman, G., Freeman, M.K., Gakidou, E., Ghosh, S., Giovannucci, E., Gmel, G., Graham, K., Grainger, R., Grant, B., Gunnell, D., Gutierrez, H.R., Hall, W., Hoek, H.W., Hogan, A., Hosgood, H.D., Hoy, D., Hu, H., Hubbell, B.J., Hutchings, S.J., Ibeanusi, S.E., Jacklyn, G.L., Jasrasaria, R., Jonas, J.B., Kan, H., Kanis, J.A., Kassebaum, N., Kawakami, N., Khang, Y.H., Khatibzadeh, S., Khoo, J.P., Kok, C., Laden, F., Lalloo, R., Lan, Q., Lathlean, T., Leasher, J.L., Leigh, J., Li, Y., Lin, J.K., Lipshultz, S.E., London, S., Lozano, R., Lu, Y., Mak, J., Malekzadeh, R., Mallinger, L., Marcenes, W., March, L., Marks, R., Martin, R., McGale, P., McGrath, J., Mehta, S., Mensah, G.A., Merriman, T.R., Micha, R., Michaud, C., Mishra, V., Hanafiah, K.M., Mokdad, A.A., Morawska, L., Mozaffarian, D., Murphy, T., Naghavi, M., Neal, B., Nelson, P.K., Nolla, J.M., Norman, R., Olives, C., Omer, S.B., Orchard, J., Osborne, R., Ostro, B., Page, A., Pandey, K.D., Parry, C.D.H., Passmore, E., Patra, J., Pearce, N., Pelizzari, P.M., Petzold, M., Phillips, M.R., Pope, D., Pope, C.A., Powles, J., Rao, M., Razavi, H., Rehfuss, E.A., Rehm, J.T., Ritz, B., Rivara, F.P., Roberts, T., Robinson, C., Rodriguez-Portales, J.A., Romieu, I., Room, R., Rosenfeld, L.C., Roy, A., Rushton, L., Salomon, J.A., Sampson, U., Sanchez-Riera, L., Sanman, E., Sapkota, A., Seedat, S., Shi, P., Shied, K., Shivakoti, R., Singh, G.M., Sleet, D.A., Smith, E., Smith, K.R., Stapelberg, N.J.C., Steenland, K., Stöckl, H., Stovner, L.J., Straif, K., Straney, L., Thurston, G.D., Tran, J.H., Van Dingenen, R., Van Donkelaar, A., Vermaan, J.L., Vijayakumar, L., Weintraub, R., Weissman, M.M., White, R.A., Whiteford, H., Wiersma, S.T., Wilkinson, J.D., Williams, H.C., Williams, W., Wilson, N., Woolf, A.D., Yip, P., Zielinski, J.M., Lopez, A.D., Murray, C.J.L., Ezzati, M., 2012.

- A comparative risk assessment of burden of disease and injury attributable to 67 risk factors and risk factor clusters in 21 regions, 1990-2010: a systematic analysis for the Global Burden of Disease Study 2010. *Lancet* 380, 2224–2260. [https://doi.org/10.1016/S0140-6736\(12\)61766-8](https://doi.org/10.1016/S0140-6736(12)61766-8).
- Lupaşcu, A., Butler, T., 2019. Source attribution of European surface O<sub>3</sub> using a tagged O<sub>3</sub> mechanism. *Atmos. Chem. Phys.* 19, 14535–14558. <https://doi.org/10.5194/acp-19-14535-2019>.
- Manders, A.M.M., Builtjes, P.J.H., Curier, L., van der Gon, H.A.C., Hendriks, C., Jonkers, S., Kranenburg, R., Kuenen, J.J.P., Segers, A.J., Timmermans, R.M.A., Visschedijk, A.J.H., Wichink Kruit, R.J., van Pul, W.A.J., Sauter, F.J., van der Swaluw, E., Swart, D.P.J., Douros, J., Eskes, H., van Meijgaard, E., van Ulft, B., van Velthoven, P., Banzhaf, S., Mues, A.C., Stern, R., Fu, G., Lu, S., Heemink, A., van Velzen, N., Schaap, M., 2017. Curriculum vitae of the LOTOS-EUROS (v2.0) chemistry transport model. *Geosci. Model Dev. (GMD)* 10, 4145–4173. <https://doi.org/10.5194/gmd-10-4145-2017>.
- Maréchal, V., Peuch, V.-H., Andersson, C., Andersson, S., Arteta, J., Beekmann, M., Benedictow, A., Bergström, R., Bessagnet, B., Cansado, A., Chêroux, F., Colette, A., Coman, A., Curier, R.L., van der Gon, H.A.C., Drouin, A., Elbern, H., Emili, E., Engelen, R.J., Eskes, H.J., Foret, G., Frieze, E., Gauss, M., Giannaros, C., Guth, J., Joly, M., Jaumouillé, E., Josse, B., Kadyrov, N., Kaiser, J.W., Krajsek, K., Kuenen, J., Kumar, U., Liora, N., Lopez, E., Malherbe, L., Martinez, I., Melas, D., Meleux, F., Menut, L., Moinat, P., Morales, T., Parmentier, J., Piacentini, A., Plu, M., Poupkou, A., Queguiner, S., Robertson, L., Rouïl, L., Schaap, M., Segers, A., Sofiev, M., Tarasson, L., Thomas, M., Timmermans, R., Valdebenito, Á., van Velthoven, P., van Versendaal, R., Vira, J., Ung, A., 2015. A regional air quality forecasting system over Europe: the MACC-II daily ensemble production. *Geosci. Model Dev. (GMD)* 8, 2777–2813. <https://doi.org/10.5194/gmd-8-2777-2015>.
- Mertens, M., Grewe, V., Rieger, V.S., Jöckel, P., 2018. Revisiting the contribution of land transport and shipping emissions to tropospheric ozone. *Atmos. Chem. Phys.* 18, 5567–5588. <https://doi.org/10.5194/acp-18-5567-2018>.
- Mues, A., Kuenen, J., Hendriks, C., Manders, A., Segers, A., Scholz, Y., Hueglin, C., Builtjes, P., Schaap, M., 2014. Sensitivity of air pollution simulations with LOTOS-EUROS to the temporal distribution of anthropogenic emissions. *Atmos. Chem. Phys.* 14, 939–955. <https://doi.org/10.5194/acp-14-939-2014>.
- Munir, S., 2016. Modelling the non-linear association of particulate matter (PM<sub>10</sub>) with meteorological parameters and other air pollutants—a case study in Makkah. *Arabian J. Geosci.* 9, 64. <https://doi.org/10.1007/s12517-015-2207-7>.
- Pommier, M., Fagerli, H., Schulz, M., Valdebenito, A., Kranenburg, R., Schaap, M., 2020. Prediction of source contributions to urban background PM<sub>10</sub> concentrations in European cities: a case study for an episode in December 2016 using EMEP/MSC-W rv4.15 and LOTOS-EUROS v2.0 - Part 1: the country contributions. *Geosci. Model Dev. (GMD)* 13. <https://doi.org/10.5194/gmd-13-1787-2020>.
- Raaschou-Nielsen, O., Andersen, Z.J., Jensen, S.S., Ketzel, M., Sørensen, M., Hansen, J., Loft, S., Tjønneland, A., Overvad, K., 2012. Traffic air pollution and mortality from cardiovascular disease and all causes: a Danish cohort study. *Environ. Heal. A Glob. Access Sci. Source*. <https://doi.org/10.1186/1476-069X-11-60>.
- Richmond-Bryant, J., Chris Owen, R., Graham, S., Snyder, M., McDow, S., Oakes, M., Kimbrough, S., 2017. Estimation of on-road NO<sub>2</sub> concentrations, NO<sub>2</sub>/NO<sub>x</sub> ratios, and related roadway gradients from near-road monitoring data. *Air Qual. Atmos. Heal.* 10, 611–625. <https://doi.org/10.1007/s11869-016-0455-7>.
- Schaap, M., Cuvelier, C., Hendriks, C., Bessagnet, B., Baldasano, J.M., Colette, A., Thunis, P., Karam, D., Fagerli, H., Graff, A., Kranenburg, R., Nyiri, A., Pay, M.T., Rouïl, L., Schulz, M., Simpson, D., Stern, R., Terrenoire, E., Wind, P., 2015. Performance of European chemistry transport models as function of horizontal resolution. *Atmos. Environ.* 112, 90–105. <https://doi.org/10.1016/j.atmosenv.2015.04.003>.
- Schaap, M., Kranenburg, R., Curier, L., Jozwicka, M., Dammers, E., Timmermans, R., 2013. Assessing the sensitivity of the OMI-NO<sub>2</sub> product to emission changes across Europe. *Rem. Sens.* 5, 4187–4208. <https://doi.org/10.3390/rs5094187>.
- Schaap, M., van Loon, M., ten Brink, H.M., Dentener, F.J., Builtjes, P.J.H., 2004. Secondary inorganic aerosol simulations for Europe with special attention to nitrate. *Atmos. Chem. Phys.* 4, 857–874. <https://doi.org/10.5194/acp-4-857-2004>.
- Schneider, C., Pelzer, M., Toenges-Schuller, N., Nacken, M., Niederrau, A., 2016. ArcGIS basierte Lösung zur detaillierten, deutschlandweiten Verteilung (Gridding) nationaler Emissionsjahreswerte auf Basis des Inventars zur Emissionsberichterstattung - Kurzfassung ; UBA TEXTE 71/2016. Für Mensch Umwelt.
- SenStadt, 2019. Luftreinhalteplan für Berlin 2. Fortschreibung (Air pollution management plan Berlin 2. Update), Berlin. Lebenswerter, Berlin.
- Thunis, P., 2018. On the validity of the incremental approach to estimate the impact of cities on air quality. *Atmos. Environ.* 173. <https://doi.org/10.1016/j.atmosenv.2017.11.012>.
- Thunis, P., Clappier, A., Pirovano, G., 2020. Source apportionment to support air quality management practices. A fitness-for-purpose guide EUR30263. <https://doi.org/10.2760/47145>. V 3.1.
- Thunis, P., Clappier, A., Tarrason, L., Cuvelier, C., Monteiro, A., Pisoni, E., Wesseling, J., Belis, C.A., Pirovano, G., Janssen, S., Guerreiro, C., Peduzzi, E., 2019. Source apportionment to support air quality planning: strengths and weaknesses of existing approaches. *Environ. Int.* <https://doi.org/10.1016/j.envint.2019.05.019>.
- Thunis, P., Degraeuwe, B., Pisoni, E., Trombetti, M., Peduzzi, E., Belis, C.A., Wilson, J., Clappier, A., Vignati, E., 2018. PM<sub>2.5</sub> source allocation in European cities: a SHERPA modelling study. *Atmos. Environ.* 187, 93–106. <https://doi.org/10.1016/j.atmosenv.2018.05.062>.
- Timmermans, R., Kranenburg, R., Hendriks, C., Thürkow, M., Kirchner, I., van Pinxteren, D., Schaap, M., 2020. Establishing the origin of particulate matter in eastern Germany using an improved regional modelling framework, 3-8. [https://doi.org/10.1007/978-3-030-22055-6\\_1](https://doi.org/10.1007/978-3-030-22055-6_1).
- Timmermans, R., Kranenburg, R., Manders, A., Hendriks, C., Segers, A., Dammers, E., Denier van der Gon, H., Schaap, M., Dammers, E., Zeng, L., Wang, L., Liu, Z., 2017. Source apportionment of PM<sub>2.5</sub> across China using LOTOS-EUROS. *Atmos. Environ.* <https://doi.org/10.1016/j.atmosenv.2017.06.003>.
- UBA, 2019. Luftqualität 2018. Für Mensch & Umwelt.
- Van Dingenen, R., Dentener, F., Crippa, M., Leitaio, J., Marmer, E., Rao, S., Solazzo, E., Valentini, L., 2018. TM5-FASST: a global atmospheric source-receptor model for rapid impact analysis of emission changes on air quality and short-lived climate pollutants. *Atmos. Chem. Phys.* 18, 16173–16211. <https://doi.org/10.5194/acp-18-16173-2018>.
- Van Zanten, M.C., Sauter, F.J., Wichink Kruit, R.J., Van Jaarsveld, J.A., Van Pul, W.A.J., 2010. Description of the DEPAC module: dry deposition modelling with DEPAC. GCN2010 ; Report 680180001/2010. RIVM, P.O. Box 1, 3720 BA Bilthoven, the Netherlands Tel +31 30 274 91 11. [www.rivm.nl](http://www.rivm.nl).
- Verstraeten, W.W., Boersma, K.F., Douros, J., Williams, J.E., Eskes, H., Liu, F., Beirle, S., Delcloo, A., 2018. Top-down NO<sub>x</sub> emissions of European cities based on the downwind plume of modelled and space-borne tropospheric NO<sub>2</sub> columns. *Sensors* 18, 1–15. <https://doi.org/10.3390/s18092893>.
- Vestreng, V., Ntziachristos, L., Semb, A., Reis, S., Isaksen, I.S.A., Tarrasón, L., 2009. Evolution of NO<sub>x</sub> and SO<sub>2</sub> emissions in Europe with focus on road transport control measures. *Atmos. Chem. Phys.* 9, 1503–1520. <https://doi.org/10.5194/acp-9-1503-2009>.
- Wagstrom, K.M., Pandis, S.N., Yarwood, G., Wilson, G.M., Morris, R.E., 2008. Development and application of a computationally efficient particulate matter apportionment algorithm in a three-dimensional chemical transport model. *Atmos. Environ.* 42, 5650–5659. <https://doi.org/10.1016/j.atmosenv.2008.03.012>.
- Walcek, C.J., 2000. Minor flux adjustment near mixing ratio extremes for simplified yet highly accurate monotonic calculation of tracer advection. *J. Geophys. Res. Atmos.* 105, 9335–9348. <https://doi.org/10.1029/1999JD901142>.
- Wang, Z.S., Chien, C.-J., Tonnesen, G.S., 2009. Development of a tagged species source apportionment algorithm to characterize three-dimensional transport and transformation of precursors and secondary pollutants. *J. Geophys. Res.* 114, D21206. <https://doi.org/10.1029/2008JD010846>.
- Whitten, G.Z., Hogo, H., Killus, J.P., 1980. The carbon-bond mechanism: a condensed kinetic mechanism for photochemical smog. *Environ. Sci. Technol.* 14, 690–700. <https://doi.org/10.1021/es60166a008>.
- Wichink Kruit, R.J., Schaap, M., Sauter, F.J., van Zanten, M.C., van Pul, W.A.J., 2012. Modeling the distribution of ammonia across Europe including bi-directional surface-atmosphere exchange. *Biogeosciences* 9, 5261–5277. <https://doi.org/10.5194/bg-9-5261-2012>.
- Zhang, L., Gong, S., Padro, J., Barrie, L., 2001. A size-segregated particle dry deposition scheme for an atmospheric aerosol module. *Atmos. Environ.* 35, 549–560. [https://doi.org/10.1016/S1352-2310\(00\)00326-5](https://doi.org/10.1016/S1352-2310(00)00326-5).